

Article

Location Information-Assisted Robust Beamforming Design for Ultra-Wideband Communication Systems

Lei Yang ¹, Zhi Zhang ¹, Xiao Fang ¹, Shiyu Cao ¹, Zhegong Shangguan ² and Shiyin Li ^{1,*}

¹ School of Information and Control Engineering, China University of Mining and Technology, Xuzhou 221116, China; yanglei94@cumt.edu.cn (L.Y.); z.zhang@cumt.edu.cn (Z.Z.); milo_fox168@163.com (X.F.); csy_cumt@cumt.edu.cn (S.C.)

² Autonomous Systems and Robotics Lab, ENSTA Paris, Institut Polytechnique de Paris, 91120 Palaiseau, France; zhegong.shangguan@ensta-paris.fr

* Correspondence: lishiyin@cumt.edu.cn

Abstract: The future of mobile communication systems is evolving rapidly toward being more intelligent, while also having the ability to interconnect with everything and be aware of the current wireless environment. For complex scenarios, the asymmetry features of channel state information (CSI) will seriously restrict the performance of the communication system. With its accurate positioning technology and high-speed communication rate, ultra-wideband (UWB) has a promising future as a solution to integrate communication and positioning functions. The traditional CSI channel estimation usually requires channel training, which will greatly increase the overhead of the system. This paper proposes a location information-assisted beamforming to replace the traditional channel training process. First, we use the user location parameter information to reconstruct the channel model and derive the CSI error distribution based on the location distribution. Second, considering the uncertainty of the user positioning error, we model the robust beamforming optimization problem that minimizes the total transmit power. To solve this non-convex problem effectively, we design a new beamforming algorithm by using semidefinite relaxation (SDR) and Bernstein-type inequalities. Finally, simulation results verify the robustness of the proposed robust beamforming compared to the worst-case robust beamforming.

Keywords: UWB; beamforming; multipath radio propagation



Citation: Yang, L.; Zhang, Z.; Fang, X.; Cao, S.; Shangguan, Z.; Li, S.

Location Information-Assisted Robust Beamforming Design for Ultra-Wideband Communication Systems. *Symmetry* **2022**, *14*, 1171.

<https://doi.org/10.3390/sym14061171>

Academic Editor: Jan Awrejcewicz

Received: 9 May 2022

Accepted: 3 June 2022

Published: 7 June 2022

Publisher's Note: MDPI stays neutral with regard to jurisdictional claims in published maps and institutional affiliations.



Copyright: © 2022 by the authors. Licensee MDPI, Basel, Switzerland. This article is an open access article distributed under the terms and conditions of the Creative Commons Attribution (CC BY) license (<https://creativecommons.org/licenses/by/4.0/>).

1. Introduction

With the development of mobile connectivity and the Internet of Things (IoT), short-range communication has attracted a lot of attention. For financial and practical reasons, it is more attractive to integrate positioning functions into existing communication technologies than to have two separate communication and positioning systems [1]. To provide better communication services for users with different channel state information, the base station (BS) needs to allocate resources asymmetrically according to different CSI [2]. However, due to information asymmetry, it is difficult to obtain the perfect status information at the base station. Therefore, this paper will obtain the user's location information through the positioning algorithm at the base station to assist beamforming. However, positioning performance in indoor environments where a global positioning system (GPS) is unavailable is necessarily affected by multipath propagation and wall obstruction. The current commonly used positioning methods, such as Bluetooth low Energy (BLE), Wi-Fi, and Zig-Bee. It is difficult to meet the communication and location needs of the next generation Internet of things mobile system. Among them, BLE and Zig-Bee technology can greatly reduce the complexity and energy consumption of system design, but their main drawback is the limited data rate [3]. The latest Wi-Fi 6 is capable of reaching a maximum data rate of 9.6 Gb/s, but it suffers from high system complexity and high power consumption, and it may not be used in scenarios with high-precision positioning requirements [4].

Ultra-wideband (UWB) technology, with its significant characteristics [5] such as high transmission rate, low power consumption, and cost-efficiency, has become an indispensable technology in the field of the Internet of Things. Based on the Shannon channel capacity theory, conventional UWB systems can achieve extremely high data transmission rates under a huge system bandwidth by transmitting very narrow Gaussian pulses [6]. For UWB positioning performance, the wide bandwidth of the UWB signal can support centimeter-level ranging accuracy and can resolve multipath delay at nanosecond resolution, so it is very suitable for short-range accurate positioning, communication, and sensing [7,8]. In addition, UWB technology possesses high robustness to multipath fading and good coexistence with other narrowband systems. UWB communication technology is a promising candidate for improving the data rate. Therefore, UWB is suitable for short-range indoor wireless communication and can be combined with cognitive radio technology, beamforming, and multiple-input multiple-output (MIMO) technology to achieve better system performance [2,9,10].

The main problem of UWB is the limited communication transmission range due to low power transmission, the multipath effect, and interference. The combination of MIMO and UWB technologies offers a feasible solution to the power limitation problem of UWB. The integration of UWB and MIMO enables wireless communication systems to increase data rates by transmitting signals over multiple channels without increasing the transmit power [11]. In indoor, dense multipath propagation environments, MIMO technology makes full use of array gain and spatial multiplexing gain to significantly improve spectral efficiency [12]. Beamforming, an important technology for MIMO, can increase the system's anti-interference capability in order to suppress interference, improve data rates, etc.

UWB beamforming is different from narrowband signal beamforming. Compared with narrowband beamforming, UWB beamforming needs fewer sensors to obtain the same angle beam, and the uniform power allocation can provide a sidelobe-free beam mode [13,14]. Through the design of a sparse array, the intercoupling between UWB antennas is effectively reduced. In [14], Wang, M. et al. proposed a time-domain beamforming algorithm that adaptively guides the array beam by estimating the direction of arrival of the signal and adjusting the corresponding time delay. Considering the nanosecond duration of the UWB pulse signal in the time domain, a least-squares-based beamforming achieved by taking full advantage of frequency invariance was proposed in [15]. Based on the geometry of the UWB antenna array, a new pointing beam was proposed to eliminate other interferences in the same frequency [16]. However, for multi-user communication systems, the performance of the proposed directional beamforming (OBF) technology was seriously degraded. A nonlinear OBF technique based on an improved radial basis function neural network was proposed in [17], which could effectively eliminate the interference caused by directional UWB. However, the array elements of the two antennas needed to be matched one by one; consequently, the implementation complexity of the system was high.

It is still worth pointing out that most of the systems designed in the literature implement communication and location functions independently, which leads to a waste of spectrum resources. At present, some researchers have paid more and more attention to location information-assisted communication, namely the use of location estimation information to improve the system capacity, thus improving the Quality of Service (QoS) of communication services [18]. The joint optimization problem of maximizing the total rate under the localization constraint and minimizing the localization error under the communication constraint was presented in a large-scale MIMO system, and the results showed that high data rate communication and mobile 3D localization can be achieved simultaneously [19]. A joint location and beamforming scheme was proposed to jointly estimate the user's position and instantaneous CSI, and then to optimize the beamforming vector according to the estimated results [20]. The existing research mainly use the estimated user location information to assist the communication process and then improve the communication quality. The common method is to take the location estimation as a constraint in order to maximize the communication rate. However, the coupling relationship between communi-

cation and location has not been considered in the existing research, and the impact of the location estimation error on CSI estimation and the communication rate has not been taken into account.

In this paper, we will make use of the inherent coupling relationship between communication rate and positioning accuracy, robust beamforming is designed by introducing CSI estimation error in the presence of multipath interference. The mechanism mainly consists of two key components. For the location, a weighted least squares (WLS) localization algorithm using reference point coordinate information is proposed. Combined with Taylor expansion and multipath information, an approximate CSI estimation error distribution is derived from the user position error distribution constructed by the Cramer–Rao Lower Bound (CRLB). On this basis, a robust beamforming optimization problem to minimize the total transmit power is formulated. Since the non-convex optimization problem is difficult to solve, a suboptimal method based on the Bernstein-type inequality and SDR is proposed. More specifically, robust beamforming is accomplished by converting the SINR probability constraint into a deterministic constraint and by transforming the unsolvable nonconvex problem into a solvable convex problem.

2. System Model

The paper considers the downlink transmission in a cellular network consisting of J cells, each having an N multi-antenna BS to transmit independent messages to one active single-antenna MS, as shown in Figure 1. It is assumed that all BSs share the same narrowband spectrum for downlink transmission. This is assuming that the exact locations of the base station (BS) and the reference node (RN) are fixed and known after their deployments. Let us denote $\mathcal{J} \triangleq \{1, 2, \dots, J\}$ as the set of the BS, the location of the j th BS is $\mathbf{u}_j = [u_{j,x}, u_{j,y}]^T$, and the location of the RN is $\mathbf{p}_f = [p_{f,x}, p_{f,y}]^T$. Each user equipment (UE) is equipped with a transmitting module for broadcasting and transmitting UWB pulse signals, and the location of the k th UE is expressed as $\mathbf{p}_k = [p_{k,x}, p_{k,y}]^T$.

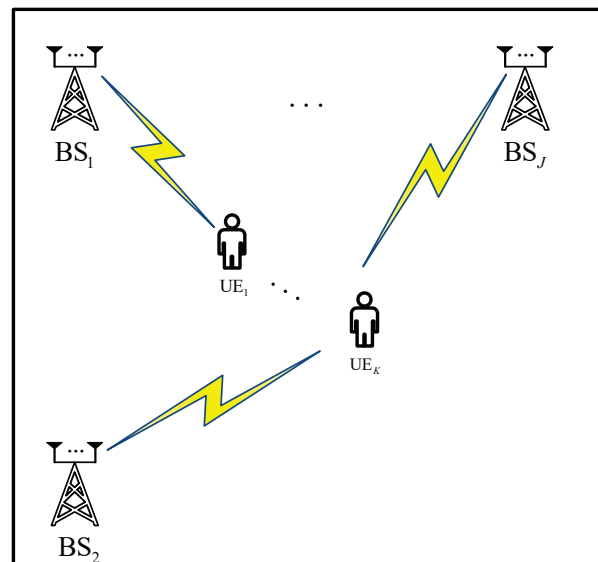


Figure 1. The considered UWB communication system model.

Each symbol is conveyed by repeating one pulse per frame (frame duration $T_f \gg T_w$) over N_f frames, resulting in a low duty cycle transmission form that is beneficial for distinguishing the multipath signal in terms of time resolution; T_w denotes each pulse

duration. The transmitted signal of this system adopts the DS-UWB modulation mode, and the transmitted symbol from the j^{th} BS to the k^{th} UE is expressed as follows [21]:

$$s_{j,k}(t) = \sum_{m=0}^{\infty} d_{j,m}^{(k)} \sum_{i=0}^{N_f-1} A_m^{(k)} p(t - mT_s - iT_f). \quad (1)$$

where $T_s = N_f T_f$ indicates the symbol duration, $d_{j,m}^{(k)}$ is the m^{th} message sent to k^{th} UE, and $A_m^{(k)} \in \{\pm 1\}$ is the spread spectrum sequence corresponding to the k^{th} UE. The second-order derivative of the Gaussian function has been widely used in practice and is used as the model of UWB signal $p(t)$. Subsequently, we will explain in detail the geometrical model, the TDOA correction method, and the CSI estimation error model.

2.1. Geometrical Model

The complex channel vector between the n^{th} antenna of the j^{th} BS and the k^{th} user is expressed as follows:

$$h_{j,k}^n(t) = \sum_{m=1}^{M-1} \beta_{jk,m}^n \delta(t - \tau_{jk,m}^n), \quad (2)$$

where $\tau_{jk,m}$ denotes the TOA of the m^{th} path between the k^{th} UE and the j^{th} BS. The complex channel fading amplitude $\beta_{jk,m}^n$ of the m^{th} path is modeled as [22]:

$$\beta_{jk,m}^n = \begin{cases} \frac{\lambda}{4\pi d_{jk,1}^n} e^{j\frac{2\pi d_{jk,1}^n}{\lambda}}, \text{ LoS}, \\ \frac{\lambda\sqrt{\Gamma_R}}{4\pi d_{jk,m}^n} e^{j\frac{2\pi d_{jk,m}^n}{\lambda}}, \text{ reflector}, \end{cases} \quad (3)$$

where Γ_R denotes the reflection coefficient, $d_{jk,1}^n = \|\mathbf{u}_j - \mathbf{p}_{k,n}\|$ denotes the direct shooting distance, $d_{jk,m}^n = \|\mathbf{a}_{jk,m} - \mathbf{p}_{k,n}\|$ denotes the distance from the j^{th} BS and the virtual point. According to the application of the image-source model for a first-order MPC, $\mathbf{a}_{jk,m}$ denotes the mirror position of the j^{th} BS on the m^{th} path, which is described in detail below.

We consider that multipath signals are reflected from the plane when the prior information of the position is known, such as walls, doors, and tables, which are represented as wall segments below [23,24]. Each wall segment $s \in \mathcal{S} = \{1, \dots, S\}$ is described by its location $\mathbf{p}_s \in \mathbb{R}^2$ (an endpoint of the wall segment) and orientation $l_s \mathbf{e}_s$, with l_s as length and the unit-vector $\mathbf{e}_s \in \mathbb{R}^2$ as the direction of the wall segment. To relate the estimated path delays to the environment, we employ a geometric model, as shown in Figure 2. The application of the image-source model for a first-order MPC is equivalent to mirroring the BS position \mathbf{u}_j at segment $s \in \mathcal{S}$, expressed as:

$$\mathbf{a}_{j,s} = \mathbf{u}_j - 2\mathbf{T}_s(\mathbf{u}_j - \mathbf{p}_s). \quad (4)$$

where $\mathbf{T}_s = \mathbf{U}_{\frac{\pi}{2}} \mathbf{e}_s \mathbf{e}_s^T \mathbf{U}_{\frac{\pi}{2}}^T$ is the rotation matrix, and $\mathbf{U}_{\frac{\pi}{2}} = \begin{bmatrix} 0 & -1 \\ 1 & 0 \end{bmatrix}$.

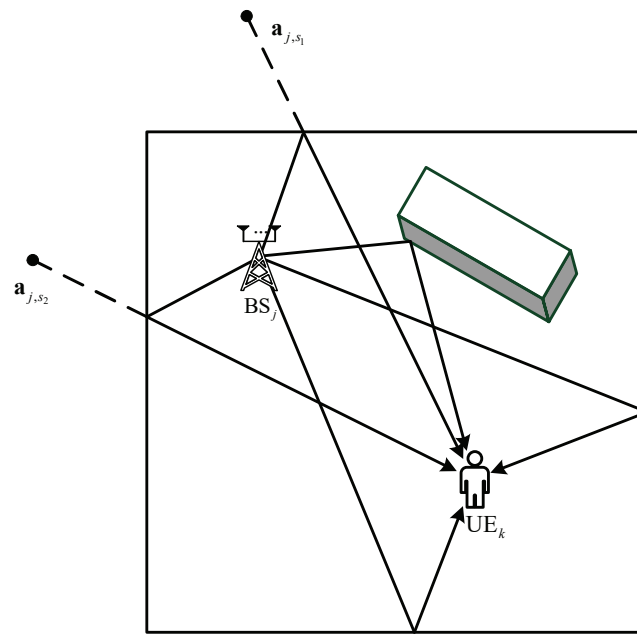


Figure 2. Illustration of multipath propagation using an image-source model.

2.2. TDOA Correction Method

In this paper, we will transmit communication and positioning signals simultaneously in the TDMA mode. Considering that the distance between the antennas is much smaller than the distance between the BS and the UE, it is reasonable to assume that the delay in arriving at each antenna of the base station is the same $\tau_{jk,m}^n = \tau_{jk,m}$. For the k th UE, the received signal vector $\mathbf{y}_k^{(p)}(t) = [y_{1,k}^{(p)}(t), \dots, y_{j,k}^{(p)}(t)]$ is expressed as follows:

$$y_{j,k}^{(p)}(t) = \sum_{m=1}^M \mathbf{h}_{jk,m} * \mathbf{w}_j s_j^{(p)}(t - \tau_{jk,m}) + n_k(t), t \in [0, T_p], \quad (5)$$

where the positioning signal of the j th BS is $s_j^{(p)}(t), t \in [0, T_p]$, $\mathbf{w}_j \in \mathbb{C}^N$ represents the beam-forming vector of the j th BS, and $\mathbf{w}_j = [w_{j,1}, \dots, w_{j,N}]^T$. $\mathbf{h}_{jk,m} \in \mathbb{C}^{1 \times N} = [\beta_{jk,m}^1, \dots, \beta_{jk,m}^N]$ represents the channel model between the j th BS and the k th UE, and $\tau_{jk,m}$ represents the TOA of the m th path. In addition, $T_p = N_p T_s$ indicates the duration of the positioning signal, and N_p denotes the number of positioning frames.

For the receiver of the UWB, the first path component (FPC) plays a very important role in finding out the receiving time of the message [25]. The received signal power is likely to be more concentrated in the FPC than in the other multipath components (MPC). In reality, UE localization is subject to equipment installation error of BS, continuous start-up errors of the UWB, and clock synchronization errors related to the external environment such as the propagation distance of pulse signals and temperature [26]. To obtain accurate real-time localization of the UE, we design a distance-corrected localization algorithm that uses RN to correct the frequency and time differences between base stations. In addition, this paper will adopt the optional bilateral two-way (AltDS-TWR) ranging mode [27]. The j th BS measures the distance from the k th UE as [28]:

$$\tilde{d}_{j,k}(t) = (1 + e_j)d_{j,k}(t) + B_j + \omega_{j,k}, \quad (6)$$

where $d_{j,k}(t)$ denotes the real distance between the j^{th} BS and k^{th} UE, e_j is the proportional error of the j^{th} BS, B_j is the measurement deviation of the j^{th} BS, and $\omega_{j,k}$ is a zero-mean

white Gaussian noise with a power spectral density N_0 . The TOA value measured by the j^{th} BS from the RN is as follows:

$$\tilde{d}_{j,f}(t) = (1 + e_j)d_{j,f}(t) + B_j + \omega_{j,f}, \quad (7)$$

where $d_{j,f}(t)$ denotes the distance between the j^{th} BS and RN. The unknown error vectors $\delta_j = [e_j \ B_j]^T$ of the j^{th} BS are estimated by the classical LS algorithm using the known coordinates of the BS and RN combined with the measured TOA data, which as follow:

$$\hat{\delta}_j = (\mathbf{F}_j^T \mathbf{F}_j)^{-1} \mathbf{F}_j^T \mathbf{f}_j, \quad (8)$$

with

$$\mathbf{F}_j = \begin{bmatrix} d_{j,f}(t) & 1 \\ d_{j,f}(t - \Delta T) & 1 \\ d_{j,f}(t - 2\Delta T) & 1 \end{bmatrix}, \mathbf{f}_j = \begin{bmatrix} \tilde{d}_{j,f}(t) - d_{j,f}(t) \\ \tilde{d}_{j,f}(t - \Delta T) - d_{j,f}(t - \Delta T) \\ \tilde{d}_{j,f}(t - 2\Delta T) - d_{j,f}(t - 2\Delta T) \end{bmatrix}, \quad (9)$$

where ΔT denotes the sample period. After obtaining the error vector of the j^{th} BS, this paper will correct the measured distance data between the k^{th} UE and the j^{th} BS in real time as follow:

$$\frac{(\tilde{d}_{j,k}(t) - \hat{B}_j)c}{1 + \hat{e}_j} = \|\mathbf{u}_j - \mathbf{p}_k(t)\| + \omega_{j,k}, \quad (10)$$

Square the two sides of (10) and subtract the equation of a common RN from the corresponding equations of the other BS, then a set of linear equations of the UE location as follow:

$$\mathbf{A}_k \mathbf{p}_k(t) = \mathbf{B}_k(t), \quad (11)$$

where

$$\mathbf{A}_k = -2 \begin{bmatrix} (\mathbf{u}_2^T - \mathbf{u}_1^T) \\ \vdots \\ (\mathbf{u}_J^T - \mathbf{u}_1^T) \end{bmatrix}, \mathbf{B}_k(t) = \begin{bmatrix} \left(\frac{\tilde{d}_{2,k}(t) - \hat{B}_2}{(1 + \hat{e}_2)} \right)^2 - \left(\frac{\tilde{d}_{1,k}(t) - \hat{B}_1}{(1 + \hat{e}_1)} \right)^2 - \mathbf{u}_2^T \mathbf{u}_2 + \mathbf{u}_1^T \mathbf{u}_1 \\ \vdots \\ \left(\frac{\tilde{d}_{J,k}(t) - \hat{B}_J}{(1 + \hat{e}_J)} \right)^2 - \left(\frac{\tilde{d}_{1,k}(t) - \hat{B}_1}{(1 + \hat{e}_1)} \right)^2 - \mathbf{u}_J^T \mathbf{u}_J + \mathbf{u}_1^T \mathbf{u}_1 \end{bmatrix}, \quad (12)$$

The classical LS localization method does not consider the effect of noise characteristics. To improve the localization accuracy, the WLS method using RN distance information will be designed, which is given by:

$$\hat{\mathbf{p}}_k(t) = (\mathbf{A}_k^T \mathbf{Q}_k \mathbf{A}_k)^{-1} (\mathbf{A}_k^T \mathbf{Q}_k \mathbf{B}_k(t)). \quad (13)$$

where \mathbf{Q}_k denotes the weighting coefficient matrix.

3. CSI Estimation Error Model

The goal of this paper is to derive an error model for CSI estimation based on the UE location and known environmental parameters. We intend to achieve this in two steps: firstly, the position error bound of UE is derived from the observed signal. Secondly, the channel error model is reconstructed under the assumption that the localization error distribution follows a Gaussian distribution [29]. After the location information of UE is obtained by the location algorithm, in order to analyze the location accuracy of UE, we will derive the CRLB of UEs to construct the location error distribution. Finally, we define the following vectors:

$$\begin{aligned} \boldsymbol{\tau}_k^T &= [\boldsymbol{\tau}_{1,k}^T, \boldsymbol{\tau}_{2,k}^T, \dots, \boldsymbol{\tau}_{J,k}^T], \\ \boldsymbol{\beta}_k^T &= [\boldsymbol{\beta}_{1,k}^T, \boldsymbol{\beta}_{2,k}^T, \dots, \boldsymbol{\beta}_{J,k}^T], \end{aligned} \quad (14)$$

where $\boldsymbol{\tau}_{j,k} = [\tau_{jk,1}, \tau_{jk,2}, \dots, \tau_{jk,M}]^T$ and $\boldsymbol{\beta}_{j,k} = [\beta_{jk,1}, \beta_{jk,2}, \dots, \beta_{jk,M}]^T$. Then, define the parameter vector of the k^{th} UE as follows:

$$\boldsymbol{\varphi}_k = [\boldsymbol{\tau}_k^T, \mathbf{R}\boldsymbol{\beta}_k^T, \mathbf{I}\boldsymbol{\beta}_k^T]^T, \tag{15}$$

where $\mathbf{R}\boldsymbol{\beta}_k \triangleq \Re\{\boldsymbol{\beta}_k\}$ and $\mathbf{I}\boldsymbol{\beta}_k \triangleq \Im\{\boldsymbol{\beta}_k\}$ represent the real and imaginary parts of the amplitude between the UE and BS, respectively. The mean square error matrix of unbiased estimation $\hat{\boldsymbol{\varphi}}_k$ satisfies the information inequality as follows [30]:

$$\mathbb{E}\{(\hat{\boldsymbol{\varphi}}_k - \boldsymbol{\varphi}_k)(\hat{\boldsymbol{\varphi}}_k - \boldsymbol{\varphi}_k)^T\} \succeq \mathbf{J}_k^{-1}, \tag{16}$$

The element of the FIM matrix $\mathbf{J}_k \in \mathbb{C}^{3JM \times 3JM}$ can be expressed as:

$$[\mathbf{J}_k]_{u,v} \triangleq \frac{1}{N_0} \int_0^{T_p} \Re\left\{ \frac{\partial \boldsymbol{\mu}_k^H(t)}{\partial \varphi_{k,u}} \frac{\partial \boldsymbol{\mu}_k(t)}{\partial \varphi_{k,v}} \right\} dt, \tag{17}$$

where $\boldsymbol{\mu}_k(t)$ is the noiseless part of the received signal in (5), given by the following equation:

$$\boldsymbol{\mu}_k(t) \triangleq \begin{bmatrix} \sum_{n=1}^N \sum_{m=1}^M \beta_{1k,m} w_{1,n} s_1^{(p)}(t - \tau_{1k,m}) \\ \vdots \\ \sum_{n=1}^N \sum_{m=1}^M \beta_{Jk,m} w_{J,n} s_J^{(p)}(t - \tau_{Jk,m}) \end{bmatrix}, \tag{18}$$

Therefore, the corresponding FIM matrix $\mathbf{J}_k \in \mathbb{C}^{3JM \times 3JM}$, partitioned into $JM \times JM$ submatrices, is structured as:

$$\mathbf{J}_k = \begin{bmatrix} \mathbf{J}_{\boldsymbol{\tau}_k, \boldsymbol{\tau}_k} & \mathbf{J}_{\boldsymbol{\tau}_k, \mathbf{R}\boldsymbol{\beta}_k} & \mathbf{J}_{\boldsymbol{\tau}_k, \mathbf{I}\boldsymbol{\beta}_k} \\ \mathbf{J}_{\boldsymbol{\tau}_k, \mathbf{R}\boldsymbol{\beta}_k}^T & \mathbf{J}_{\mathbf{R}\boldsymbol{\beta}_k, \mathbf{R}\boldsymbol{\beta}_k} & \mathbf{J}_{\mathbf{R}\boldsymbol{\beta}_k, \mathbf{I}\boldsymbol{\beta}_k} \\ \mathbf{J}_{\boldsymbol{\tau}_k, \mathbf{I}\boldsymbol{\beta}_k}^T & \mathbf{J}_{\mathbf{I}\boldsymbol{\beta}_k, \mathbf{R}\boldsymbol{\beta}_k} & \mathbf{J}_{\mathbf{I}\boldsymbol{\beta}_k, \mathbf{I}\boldsymbol{\beta}_k} \end{bmatrix}, \tag{19}$$

Each submatrix in (19) is expressed as follows:

$$\begin{aligned} \mathbf{J}_{\boldsymbol{\tau}_k, \boldsymbol{\tau}_k} &= \text{diag}\{\mathbf{J}_{\boldsymbol{\tau}_{1k}, \boldsymbol{\tau}_{1k}}, \dots, \mathbf{J}_{\boldsymbol{\tau}_{Jk}, \boldsymbol{\tau}_{Jk}}\}, \\ \mathbf{J}_{\boldsymbol{\tau}_k, \mathbf{R}\boldsymbol{\beta}_k} &= \text{diag}\{\mathbf{J}_{\boldsymbol{\tau}_{1k}, \mathbf{R}\boldsymbol{\beta}_{1k}}, \dots, \mathbf{J}_{\boldsymbol{\tau}_{Jk}, \mathbf{R}\boldsymbol{\beta}_{Jk}}\}, \\ \mathbf{J}_{\boldsymbol{\tau}_k, \mathbf{I}\boldsymbol{\beta}_k} &= \text{diag}\{\mathbf{J}_{\boldsymbol{\tau}_{1k}, \mathbf{I}\boldsymbol{\beta}_{1k}}, \dots, \mathbf{J}_{\boldsymbol{\tau}_{Jk}, \mathbf{I}\boldsymbol{\beta}_{Jk}}\}, \\ \mathbf{J}_{\mathbf{R}\boldsymbol{\beta}_k, \mathbf{R}\boldsymbol{\beta}_k} &= \text{diag}\{\mathbf{J}_{\mathbf{R}\boldsymbol{\beta}_{1k}, \mathbf{R}\boldsymbol{\beta}_{1k}}, \dots, \mathbf{J}_{\mathbf{R}\boldsymbol{\beta}_{Jk}, \mathbf{R}\boldsymbol{\beta}_{Jk}}\}, \\ \mathbf{J}_{\mathbf{I}\boldsymbol{\beta}_k, \mathbf{I}\boldsymbol{\beta}_k} &= \text{diag}\{\mathbf{J}_{\mathbf{I}\boldsymbol{\beta}_{1k}, \mathbf{I}\boldsymbol{\beta}_{1k}}, \dots, \mathbf{J}_{\mathbf{I}\boldsymbol{\beta}_{Jk}, \mathbf{I}\boldsymbol{\beta}_{Jk}}\}, \end{aligned} \tag{20}$$

where $\mathbf{J}_{\boldsymbol{\tau}_{jk}, \boldsymbol{\tau}_{jk}} \in \mathbb{C}^{M \times M}$, $\mathbf{J}_{\boldsymbol{\tau}_{jk}, \mathbf{R}\boldsymbol{\beta}_{jk}} \in \mathbb{C}^{M \times M}$, $\mathbf{J}_{\boldsymbol{\tau}_{jk}, \mathbf{I}\boldsymbol{\beta}_{jk}} \in \mathbb{C}^{M \times M}$, $\mathbf{J}_{\mathbf{I}\boldsymbol{\beta}_{1k}, \mathbf{I}\boldsymbol{\beta}_{1k}} \in \mathbb{C}^{M \times M}$, and $\mathbf{J}_{\mathbf{I}\boldsymbol{\beta}_{1k}, \mathbf{I}\boldsymbol{\beta}_{1k}} \in \mathbb{C}^{M \times M}$ are denoted as:

$$\begin{aligned} \mathbf{J}_{\mathbf{R}\boldsymbol{\beta}_{jk}, \mathbf{R}\boldsymbol{\beta}_{jk}} &= \mathbf{J}_{\mathbf{I}\boldsymbol{\beta}_{jk}, \mathbf{I}\boldsymbol{\beta}_{jk}} = \frac{N_p}{N_0} \left(\sum_{n=1}^N w_{j,n} \right)^2 \Re\{\mathbf{R}_0\}, \\ \mathbf{J}_{\mathbf{R}\boldsymbol{\beta}_{jk}, \mathbf{I}\boldsymbol{\beta}_{jk}} &= j \frac{N_p}{N_0} \left(\sum_{n=1}^N w_{j,n} \right)^2 \Re\{\mathbf{R}_0\}, \\ \mathbf{J}_{\boldsymbol{\tau}_{jk}, \boldsymbol{\tau}_{jk}} &= \frac{N_p}{N_0} \left(\sum_{n=1}^N w_{j,n} \right)^2 \Re\{\mathbf{B}_k^H \mathbf{R}_2 \mathbf{B}_k\}, \\ \mathbf{J}_{\boldsymbol{\tau}_{jk}, \mathbf{R}\boldsymbol{\beta}_{jk}} &= \frac{N_p}{N_0} \left(\sum_{n=1}^N w_{j,n} \right)^2 \Re\{\mathbf{R}_1 \mathbf{B}_k\}, \end{aligned} \tag{21}$$

where $\mathbf{B}_k = \text{diag}\{\beta_k\}$; for details, see Appendix A. Assuming that the symbols are independent and identically distributed, the matrix \mathbf{R}_i elements are expressed as follows:

$$[\mathbf{R}_i]_{u,v} \triangleq \int_{-W/2}^{W/2} (2\pi f)^i |P(f)|^2 e^{-j2\pi f \Delta\tau_{u,v}} df, \quad (22)$$

in which $\Delta\tau_{u,v} = \tau_{jk,u} - \tau_{jk,v}$, $i = \{0, 1, 2\}$, and W is the signal bandwidth. As can be seen from the formula above, when i is 0 or 2, the diagonal element of \mathbf{R}_0 and \mathbf{R}_2 is the largest 1 and $4\pi^2 W_{\text{eff}}^2$, respectively, and $W_{\text{eff}}^2 = \int_{-W/2}^{W/2} f^2 |P(f)|^2 df$ is the effective bandwidth. In addition, for any bandwidth W , $\text{diag}(\mathbf{R}_1) = \mathbf{0}_M$, $\lim_{W \rightarrow \infty} \mathbf{R}_1 = \mathbf{0}_{M \times M}$. In order to directly calculate the CRLB of the UE position, it is necessary to redefine the unknown parameter vector according to the chain rule, and the equivalent Fisher matrix of the position can be expressed as follows [28]:

$$\mathbf{J}_{\mathbf{p}_k} = \mathbf{b}_k^H \mathbf{J}_{\tau_k \tau_k} \mathbf{b}_k, \quad (23)$$

where the elements of the vector $\mathbf{b}_k \in \mathbb{R}^{JM \times 1}$ are expressed as:

$$[\mathbf{b}_k]_n = \frac{\mathbf{p}_k - \mathbf{a}_{j_n, k, m_n}}{c \|\mathbf{p}_k - \mathbf{a}_{j_n, k, m_n}\|_2}. \quad (24)$$

where \mathbf{a}_{j_n, k, m_n} denotes the reflection point coordinates of the m^{th} from the j^{th} BS for the k^{th} UE, where m_n and j_n are related to n , respectively, by $j_n = \lfloor n/M \rfloor$, $m_n = n \bmod M$.

According to the reference point auxiliary location algorithm proposed in the previous section, the location $\hat{\mathbf{p}}_k(t)$ of the UE can be estimated in real time, but in practice, due to the BS coordinate error and measurement error, it is impossible for the estimation algorithm to obtain accurate UE coordinates. The estimation error at this time is expressed as $\mathbf{e}_k(t) = \mathbf{p}_k(t) - \hat{\mathbf{p}}_k(t)$. Considering the assumption of Gaussian white noise, the least square equivalent and maximum likelihood estimation method can achieve the estimation result under CRLB; that is, the positioning error \mathbf{e}_k obeys the mean value $\mathbf{0}$, while the variance is $\mathbf{J}_{\mathbf{p}_k}^{-1}$.

$$\mathbf{e}_{\mathbf{p}_k}(t) \sim \mathcal{CN}(\mathbf{0}, \mathbf{J}_{\mathbf{p}_k}^{-1}), \quad (25)$$

with the location of the k^{th} UE and the known environmental parameters, the partial channel model $\hat{\beta}_{jk,m}(t)$ between the k^{th} UE and the j^{th} BS can be constructed, and its elements are expressed as $\hat{\beta}_{jk,m}(t) = [\hat{\beta}_{jk,m}^1(t), \dots, \hat{\beta}_{jk,m}^N(t)]$. The channel estimation error is expressed as follows:

$$\Delta\beta_{jk,m}^n(t) \approx \begin{cases} \frac{\lambda}{4\pi} \frac{(\hat{\mathbf{p}}_k(t) - \mathbf{u}_{j,n})^T \mathbf{e}_k(t)}{\|\hat{\mathbf{p}}_k(t) - \mathbf{u}_j\|_2^3}, & m = 1 \\ \frac{\lambda \sqrt{\Gamma_R} (\hat{\mathbf{p}}_k(t) - \mathbf{u}_{j,n})^T \mathbf{e}_k(t)}{4\pi (\|\hat{\mathbf{p}}_k(t) - \mathbf{a}_{k,m}\|_2 + \|\mathbf{a}_{k,m} - \mathbf{u}_j\|_2)^3}, & m \geq 2 \end{cases} \quad (26)$$

Furthermore, this paper uses the first-order Taylor expansion formula, given by the following equation:

$$\|\hat{\mathbf{p}}_k(t) + \mathbf{e}_k(t) - \mathbf{u}_j\|_2 \approx \|\hat{\mathbf{p}}_k(t) - \mathbf{u}_j\|_2 - \frac{(\hat{\mathbf{p}}_k(t) - \mathbf{u}_j)^T}{\|\hat{\mathbf{p}}_k(t) - \mathbf{u}_j\|_2} \mathbf{e}_k(t). \quad (27)$$

4. Robust Beamforming

This section is based on the estimated position of k^{th} UE for beamforming. The distance between the UE and all BSs is first calculated, and then the closest base station is selected for communication services. For the convenience of representation, we consider

the j th UE and the j th base station to be the closest. The received signal of the j th UE is represented by the following equation:

$$y_j^{(c)}(t) = \sum_{m=1}^M (\hat{\beta}_{jj,m} + \Delta\beta_{jj,m}) * \mathbf{w}_j s_j^{(c)}(t - \tau_{jj,m}) + \sum_{i \neq j}^J \sum_{m=1}^M (\hat{\beta}_{ij,m} + \Delta\beta_{ij,m}) * \mathbf{w}_i s_i^{(c)}(t - \tau_{ij,m}) + n_j(t), t \in [T_p, T_p + T_c], \tag{28}$$

where $s_j^{(c)}(t)$ denotes the communication signal of the j th BS, and T_c is the communication duration. The rate of the j th UE served by the j th BS is expressed as follows:

$$R_j = \frac{T_c}{T_p + T_c} \log \left(1 + \frac{|\hat{\mathbf{g}}_{jj} + \Delta\mathbf{g}_{jj} \mathbf{w}_j|^2}{\left| \sum_{i \neq j}^J (\hat{\mathbf{g}}_{ij} + \Delta\mathbf{g}_{ij}) \mathbf{w}_i \right|^2 + \sigma_j^2} \right), \tag{29}$$

where $\hat{\mathbf{g}}_{jj} = \sum_{m=1}^M \hat{\beta}_{jj,m} \mathbf{e}_j$, $\Delta\mathbf{g}_{jj} = \sum_{m=1}^M \Delta\beta_{jj,m} \mathbf{e}_j$. The n th element of $\Delta\mathbf{g}_{jj}$ is represented by $\Delta g_{jj,n} = \mathbf{b}_{jj,n}^T \mathbf{e}_j$, with:

$$\mathbf{b}_{jj,n} = \left(\frac{\lambda}{4\pi} \left(\frac{(\hat{\mathbf{p}}_j - \mathbf{u}_{j,n})}{\|\hat{\mathbf{p}}_j - \mathbf{u}_{j,n}\|_2^3} \right) + \sum_{m=2}^M \frac{\lambda \sqrt{\Gamma_R} (\hat{\mathbf{p}}_j - \mathbf{u}_{j,m})}{4\pi (\|\hat{\mathbf{p}}_j - \mathbf{a}_j\|_2 + \|\mathbf{a}_j - \mathbf{u}_{j,m}\|_2)^3} \right), \tag{30}$$

Each BS is scattered throughout the coverage area according to certain rules. When the BS receives the positioning data signal from the UE, it is connected to the central processing unit through high-speed transmission media such as optical fiber. The robust beamforming optimization problem to minimize the total transmit power is formulated as follows:

$$\begin{aligned} \min_{\{\mathbf{w}_j\}_{j=1}^J} & \sum_{j=1}^J \|\mathbf{w}_j\|_2^2 \\ \text{s.t.} & \|\mathbf{w}_j\|_2^2 \leq p_{\text{UWB}}^{\max}, j = 1, \dots, J, \\ & \Pr\{\text{SINR}_j(\Delta\mathbf{g}_{jj}^H) \leq \gamma_j\} \leq \rho_j, \end{aligned} \tag{31}$$

where p_{UWB}^{\max} represents the maximum power, $\gamma_j = 2^{(T_p+T_c)\bar{R}/T_c} - 1$ denotes the minimum SINR constraint of the j th UE and the maximum outage probability ρ_j of the j th UE. We define $\mathbf{W}_j \triangleq \mathbf{w}_j \mathbf{w}_j^H$. To simplify the calculation, the SINR of the j th BS is expressed as follows:

$$f(\Delta\mathbf{g}_{jj}) = \hat{\mathbf{g}}_{jj}^H \mathbf{W}_j \hat{\mathbf{g}}_{jj} + 2\text{Re}\left\{ \Delta\mathbf{g}_{jj}^H \mathbf{W}_j \hat{\mathbf{g}}_{jj} \right\} + \Delta\mathbf{g}_{jj}^H \mathbf{W}_j \Delta\mathbf{g}_{jj}, \tag{32}$$

Therefore, the constraint (31) of the optimization problem is represented by the following equation:

$$\Pr\left\{ \frac{f(\Delta\mathbf{g}_{jj})}{\gamma_j} - \sum_{i=1, i \neq j}^J f(\Delta\mathbf{g}_{ij}) \leq \sigma_j^2 \right\} \leq p_{\text{out}}, \tag{33}$$

According to formula (25), the signal amplitude error is expressed as:

$$\Delta\mathbf{g}_{jj} \sim \mathcal{CN}(0, \Delta\mathbf{B}_{jj}^T \Delta\mathbf{B}_{jj} \mathbf{J}_{\mathbf{p}_k}^{-1}), \tag{34}$$

where $\Delta \mathbf{B}_{jj} \in \mathbb{R}^{N \times 2}$, $\Delta \mathbf{B}_{jj} = [b_{jj,1}^T, \dots, b_{jj,N}^T]^T$. The signal amplitude error is rewritten as:

$$\Delta \mathbf{g}_{jj} = \mathbf{E}_{jj} \mathbf{v}_j, \quad (35)$$

where $\mathbf{v}_j \sim \mathcal{N}(0, \mathbf{I})$, $\mathbf{E}_{jj} = \sqrt{\Delta \mathbf{B}_{jj}^H \Delta \mathbf{B}_{jj} \mathbf{J}_{\mathbf{p}_j}^{-1}}$. In order to simplify the equation, we defined $\bar{\mathbf{E}}_j = \text{diag}\{\mathbf{E}_{1,j}, \dots, \mathbf{E}_{J,j}\}$ and $\bar{\mathbf{g}}_j = [\mathbf{g}_{1,j}^T, \dots, \mathbf{g}_{J,j}^T]^T$. Then, we can obtain the following equation:

$$\Delta \bar{\mathbf{g}}_j = \bar{\mathbf{E}}_j \bar{\mathbf{g}}_j, \quad (36)$$

where

$$\begin{aligned} \Delta \bar{\mathbf{g}}_j &= [\Delta \mathbf{g}_{1,j}^T, \dots, \Delta \mathbf{g}_{J,j}^T]^T, \\ \bar{\mathbf{W}}_j &= \text{diag}\{-\mathbf{W}_1, \dots, -\mathbf{W}_{j-1}, \frac{\mathbf{W}_j}{\gamma_j}, -\mathbf{W}_{j+1}, \dots, -\mathbf{W}_J\}, \end{aligned} \quad (37)$$

then

$$\frac{f(\Delta \beta_{jj})}{\gamma_j} - \sum_{i=1, i \neq j}^J f(\Delta \beta_{ij}) = \bar{\mathbf{v}}_j^T \bar{\mathbf{A}}_j \bar{\mathbf{v}}_j^* + 2\text{Re}\{\bar{\mathbf{v}}_j^T \bar{\mathbf{a}}_j\} + \bar{\mathbf{g}}_j^T \bar{\mathbf{W}}_j \bar{\mathbf{g}}_j^*, \quad (38)$$

where

$$\bar{\mathbf{A}}_j = \bar{\mathbf{E}}_j \odot \bar{\mathbf{W}}_j \odot \bar{\mathbf{E}}_j, \bar{\mathbf{a}}_j = \bar{\mathbf{E}}_j \odot \bar{\mathbf{W}}_j \bar{\mathbf{g}}_j, \quad (39)$$

where \odot denotes the Hadamard product. Therefore, the constraint item (31) can be expressed as:

$$\Pr\{\bar{\mathbf{v}}_j^T \bar{\mathbf{A}}_j \bar{\mathbf{v}}_j^* + 2\text{Re}\{\bar{\mathbf{v}}_j^T \bar{\mathbf{a}}_j\} \leq c_j\} \leq \rho_j, \quad (40)$$

where $c_j = \sigma_j^2 - \bar{\mathbf{g}}_j^T \bar{\mathbf{W}}_j \bar{\mathbf{g}}_j^*$. In order to transform probabilistic constraints into deterministic constraints, this paper uses the following Bernstein-type inequalities: $\mathbf{G} = \mathbf{v}^H \mathbf{A} \mathbf{v} + 2\mathbf{v}^H \mathbf{a}$, $\mathbf{A} \in \mathbb{H}^N$, $\mathbf{a} \in \mathbb{C}^N$, $\mathbf{v} \sim \mathcal{CN}(0, \mathbf{I})$. For any $\zeta > 0$, the following inequality holds:

$$\Pr\{\mathbf{G} \leq \text{Tr}(\mathbf{A}) - \sqrt{2\zeta} \sqrt{\|\text{vec}(\mathbf{A})\|^2 + 2\|\mathbf{a}\|^2} - \zeta s^-(\mathbf{A})\} \leq \exp(-\zeta), \quad (41)$$

where $s^-(\mathbf{A}) = \max\{\lambda_{\max}(-\mathbf{A}), 0\}$, $s^+(\mathbf{A}) = \max\{\lambda_{\max}(\mathbf{A}), 0\}$, $\lambda_{\max}(\mathbf{A})$ is the largest eigenvalue of matrix \mathbf{A} . According to the Bernstein-type inequality, the constraint term (33) is the following deterministic constraint:

$$\text{Tr}(\bar{\mathbf{A}}_j) - \sqrt{2\zeta_j} \sqrt{\|\text{vec}(\bar{\mathbf{A}}_j)\|^2 + 2\|\bar{\mathbf{a}}_j\|^2} - \zeta_j s^-(\bar{\mathbf{A}}_j) \geq c_j, \quad (42)$$

where $\zeta_j = -\ln(\rho_j)$. Furthermore, the constraints of (42) can be reformulated as:

$$\text{Tr}(\bar{\mathbf{A}}_j) - \sqrt{2\zeta_j} \mu_j - \zeta_j v_j - c_j \geq 0, \forall j \in \mathcal{J}, \quad (43a)$$

$$\|\text{vec}(\bar{\mathbf{A}}_j), \sqrt{2}\bar{\mathbf{a}}_j\| \leq \mu_j, \forall j \in \mathcal{J}, \quad (43b)$$

$$v_j \mathbf{I}_{j \times j} + \bar{\mathbf{A}}_j \geq \mathbf{0}, v_j \geq 0, \forall j \in \mathcal{J}, \quad (43c)$$

where μ_j and v_j represent a relaxation variable. We have transformed the second non-convex constraint of formula (31) into the convex constraints 43a, 43b, 43c, so that problem (31) can be effectively solved by the convex optimization tool: CVX.

5. Simulation Results

In this section, the performance of the proposed location information-assisted method is verified by simulation, and the effect of the number of antennas, SINR threshold, and room size on the proposed robust power allocation is analyzed. Assuming that $J = 6$, $N = 5$, $K = 4$, the reflection coefficient $\Gamma_R = 0.7$. The probability of the constraints are set to 0.05, i.e., $\rho_j = 0.05, \forall j$.

The SINR generated by 5000 random channels is summarized as a cumulative distribution function (CDF) in Figure 3. It can be seen in Figure 3 that the CDF rate of the non-robust power distribution cannot guarantee the minimum rate requirement, while the proposed robust power distribution satisfies the minimum rate constraint. In the non-robust beamforming method, there is no way to always assign extra power to users to suppress interference from other users; therefore, it is difficult for SINR to maintain at a certain level. However, the robust method proposed can allocate a reasonable amount of power to the users in order to improve the signal-to-noise ratio, thus the SINR value is always greater than the threshold value.

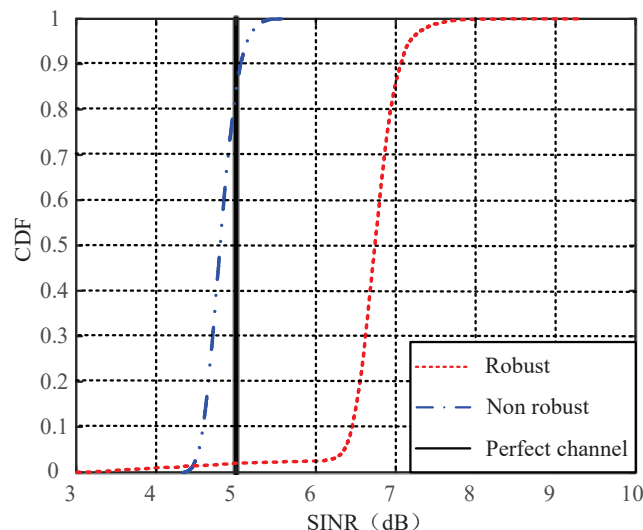


Figure 3. CDF rate of over 5000 random channel realizations.

In order to demonstrate the performance of the proposed robust beamforming method, we compare the performance with the non-robust beamforming method (which ignores the estimation errors) and the worst-case scheme (which is presented in [31]). The variation curve of the average transmit power with the SINR threshold in the robust, non-robust, and worst-case is shown in Figure 4. Compared with the non-robust power allocation, robust power allocation requires more power to maintain the SINR at a stable level. In addition, compared with the worst-case robust beamforming, the proposed method yields less conservative results.

Figure 5 analyzes the situation in different scene sizes. It can be seen that as the room size becomes larger, the transmit power for both the robust and the non-robust beamforming gradually becomes larger. Since this paper assumes that the BSs are mainly arranged in the four corners of the scene, the measurement distance error between the BSs and the UE inevitably increases as the scene size increases, which leads to both robust beamforming and non-robust beamforming that require more power to cope with the channel error.

Figure 6 gives the average transmit power versus the transmit antenna number. As the number of antennas increases, the power required for the non-robust, robust, and worst-case scenarios gradually decreases. We can see that the method is more effective than the worst-case method, and therefore the method is less conservative. In addition, from the Equation (21), the CRLB of the user location is inversely proportional to the antenna number. Increasing the antennas number not only improves the accuracy of the user location but also improves the reliability of the reconstructed channel.

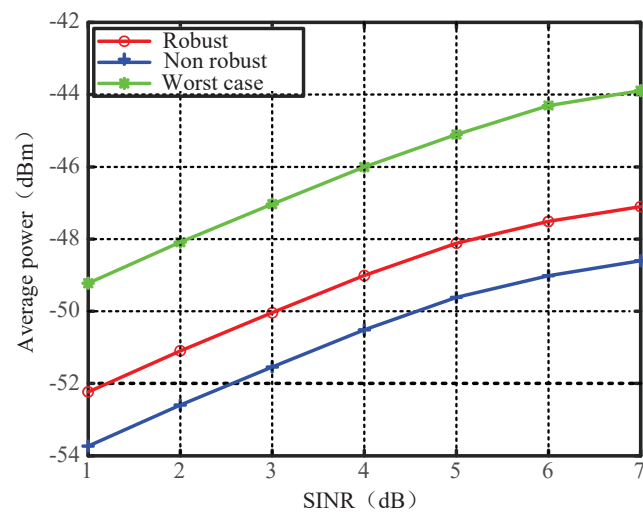


Figure 4. Average transmit power versus the SINR γ (dB).

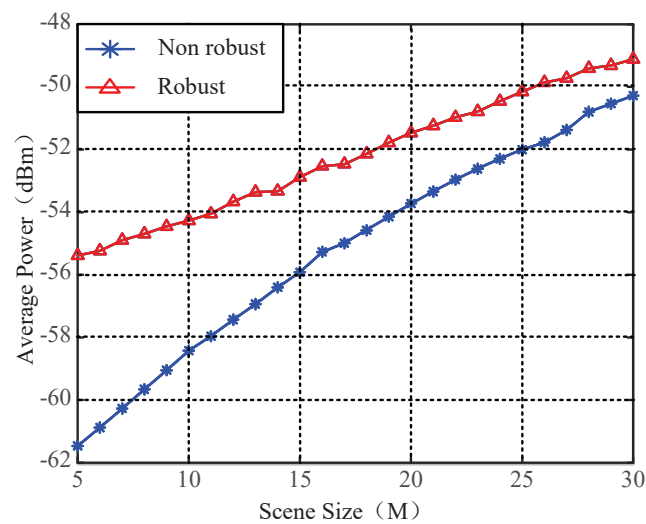


Figure 5. Average transmit power versus the scene size.

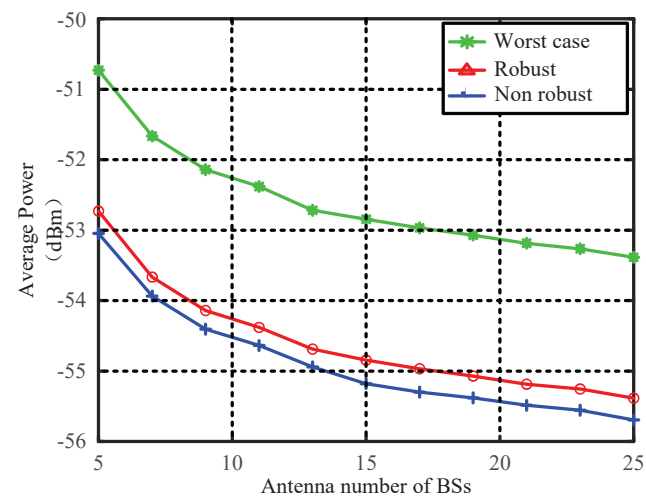


Figure 6. Average transmit power versus the antenna number.

6. Conclusions

In this paper, we derived the CSI error bounded in the case of UE location uncertainty, with the help of the Taylor approximation, when using the estimated UE position to obtain the CSI in UWB wireless communication systems. Then, to resist the impact of the position error on the beamforming design, we proposed a robust beamforming optimization problem to minimize the total transmit power. To efficiently solve this nonconvex problem, we proposed an SDR-based algorithm and evaluated the performance of the UE in terms of SINR, scene size, and the antenna number. The simulation results verify the theoretical derivation of the CSI error bound, and the robustness of the method was verified by its comparison with the worst-case and non-robust methods. Therefore, the beamforming scheme proposed in this paper can have a good application prospect in promoting the development of location information-assisted UWB communication.

Author Contributions: Conceptualization, L.Y. and S.L.; software, Z.Z., X.F., and Z.S.; writing—review and editing, L.Y. and S.C.; formal analysis, S.L.; funding acquisition, S.L. All authors have read and agreed to the published version of the manuscript.

Funding: This research was funded by the National Natural Science Foundation of China under Grant 61771474.

Institutional Review Board Statement: Not applicable.

Informed Consent Statement: Not applicable.

Data Availability Statement: Not applicable.

Acknowledgments: The authors would like to thank the editors and the reviewers for their helpful suggestions and constructive comments.

Conflicts of Interest: The authors declare no conflict of interest.

Appendix A

Taking the derivative of (18) with respect to the unknown parameters, we can write the following equation:

$$\begin{aligned} \left[\frac{\partial \mu_f}{\partial \tau_{jk,m}} \right]_j &= \sum_{n=1}^N \beta_{jk,m} w_{1,n} \frac{\partial s_k^U(t - \tau_{jk,m})}{\partial \tau_{jk,m}}, \\ \left[\frac{\partial \mu_f}{\partial R \beta_{jk,m}} \right]_j &= -j \left[\frac{\partial \mu_f}{\partial R \beta_{jk,m}} \right]_j = \sum_{n=1}^N w_{j,n} s_k^U(t - \tau_{jk,m}), \end{aligned} \tag{A1}$$

Therefore, the submatrix of FIM can be expressed as follows:

$$[\mathbf{J}_{\tau_{jk} \tau_{jk}}]_{u,v} = \frac{1}{N_0} \Re \left\{ N^2 N_s \beta_{jk,u} \beta_{jk,v} [\mathbf{R}_2]_{u,v} \right\}, \tag{A2}$$

where

$$\begin{aligned} [\mathbf{R}_2]_{u,v} &\triangleq \int_0^{T_o} \frac{\partial s_k^*(t - \tau_{jk,u})}{\partial \tau_{jk,u}} \frac{\partial s_k(t - \tau_{jk,v})}{\partial \tau_{jk,v}} dt \\ &= \int_{-W/2}^{W/2} (2\pi f)^2 |P(f)|^2 e^{-j2\pi f \Delta \tau_{uv}} df, \end{aligned} \tag{A3}$$

We can rewrite $\mathbf{J}_{\tau_{jk} \tau_{jk,u}}$ as:

$$\mathbf{J}_{\tau_{j,k} \tau_{j,k}} = \frac{N_s}{N_0} \left(\sum_{n=1}^N w_{j,n} \right)^2 \Re \{ \mathbf{B}^H \mathbf{R}_2 \mathbf{B} \}. \tag{A4}$$

The other submatrices of (21) can be obtained similarly.

References

1. Cui, Y.; Liu, F.; Jing, X.; Mu, J. Integrating Sensing and Communications for Ubiquitous IoT: Applications, Trends, and Challenges. *IEEE Netw.* **2021**, *35*, 158–167. [CrossRef]
2. Fanti, A.; Schirru, L.; Casu, S.; Lodi, M.B.; Riccio, G.; Mazzarella, G. Improvement and Testing of Models for Field Level Evaluation in Urban Environment. *IEEE Trans. Antennas Propag.* **2021**, *68*, 4038–4047. [CrossRef]
3. Decuir, J. Bluetooth Smart Support for 6LoBTLE: Applications and connection questions. *IEEE Consum. Electron. Mag.* **2015**, *4*, 67–70. [CrossRef]
4. Naik, G.; Park, J.; Ashdown, J.; Lehr, W. Next Generation Wi-Fi and 5G NR-U in the 6 GHz Bands: Opportunities and Challenges. *IEEE Access* **2020**, *8*, 153027–153056. [CrossRef]
5. Gezici, S.; Poor, H.V. Position estimation via ultra-wide-band signals. *Proc. IEEE* **2009**, *97*, 386–403. [CrossRef]
6. Win, M.; Scholtz, R. Ultra-wide bandwidth time-hopping spread spectrum impulse radio for wireless multiple-access communications. *IEEE Trans. Commun.* **2000**, *48*, 679–691. [CrossRef]
7. Zhu, X.; Yi, J.; Cheng, J.; He, L. Adapted Error Map Based Mobile Robot UWB Indoor Positioning. *IEEE Trans. Instrum. Meas.* **2020**, *69*, 6336–6350. [CrossRef]
8. Fang, Z.; Wang, W.; Wang, J.; Liu, B.; Tang, K.; Lou, L.; Heng, C.; Wang, C.; Zheng, Y. Integrated Wideband Chip-Scale RF Transceivers for Radar Sensing and UWB Communications: A Survey. *IEEE Circuits Syst. Mag.* **2022**, *22*, 40–76. [CrossRef]
9. Zhang, S.; Pedersen, G.F. Mutual Coupling Reduction for UWB MIMO Antennas With a Wideband Neutralization Line. *IEEE Antennas Wirel. Propag. Lett.* **2016**, *15*, 166–169. [CrossRef]
10. Kaiser, T.; Zheng, F.; Dimitrov, E. An Overview of Ultra-Wide-Band Systems With MIMO. *Proc. IEEE* **2009**, *97*, 285–312. [CrossRef]
11. Drobczyk, M.; Lehmann, M.; Strowik, C. EMC characterization of the UWB-based wireless positioning and communication experiment (wireless Compose) for the ISS. In Proceedings of the 2017 IEEE International Conference on Wireless for Space and Extreme Environments (WiSEE), Montreal, QC, Canada, 10–12 October 2017.
12. Schirru, L.; Ledda, F.; Lodi, M.B.; Fanti, A.; Mannaro, K.; Ortu, M.; Mazzarella, G. Electromagnetic Field Levels in Built-up Areas with an Irregular Grid of Buildings: Modeling and Integrated Software. *Electronics* **2020**, *9*, 765. [CrossRef]
13. Hussain, M.G.M. Principles of space-time array processing for ultrawide-band impulse radar and radio communications. *IEEE Trans. Veh. Technol.* **2002**, *51*, 393–403. [CrossRef]
14. Wang, M.; Yang, S.; Wu, S. Beamforming of UWB pulse array and its implementation. *Digit. Signal Process.* **2006**, *16*, 333–342. [CrossRef]
15. Zebiri, C.; Benabdelaziz, F.; Lashab, M. Beamforming of ultra wideband signals in an IEEE 802.15.3a channel environment. In Proceedings of the 2014 IEEE International Conference on Ultra-WideBand (ICUWB), Paris, France, 1–3 September 2014.
16. Aye, S.; Ng, B.P. Introduction to a New Array Processing Concept: Orientational Beamforming. *IEEE Commun. Mag.* **2019**, *57*, 51–57. [CrossRef]
17. Han, J.; Ng, B.P.; Er, M.H. Orientational Beamforming via a Modified RBF Neural Network for Orientational UWB Interference Rejection. *IEEE Trans. Veh. Technol.* **2022**, *71*, 2900–2913. [CrossRef]
18. Hu, X.; Zhong, C.; Zhang, Y.; Chen, X.; Zhang, Z. Location Information Aided Multiple Intelligent Reflecting Surface Systems. *IEEE Trans. Commun.* **2020**, *68*, 7948–7962. [CrossRef]
19. Jeong, S.; Simeone, O.; Kang, J. Optimization of Massive Full-Dimensional MIMO for Positioning and Communication. *IEEE Trans. Wirel. Commun.* **2018**, *17*, 6205–6217. [CrossRef]
20. Zhou, B.; Liu, A.; Lau, V. Successive localization and beamforming in 5G mmWave MIMO communication systems. *IEEE Trans. Signal Process.* **2019**, *67*, 1620–1635. [CrossRef]
21. Parihar, A.; Lampe, L.; Schober, R.; Leung, C. Equalization for DS-UWB Systems—Part I: BPSK Modulation. *IEEE Trans. Commun.* **2007**, *55*, 1164–1173. [CrossRef]
22. Abu-Shaban, Z.; Zhou, X.; Abhayapala, T.; Seco-Granados, G.; Wymeersch, H. Error Bounds for Uplink and Downlink 3D Localization in 5G Millimeter Wave Systems. *IEEE Trans. Wirel. Commun.* **2018**, *17*, 4939–4954. [CrossRef]
23. Kulmer, J.; Leitinger, E.; Meissner, P.; Hinteregger, S.; Witrisal, K. Cooperative localization and tracking using multipath channel information. In Proceedings of the 2016 International Conference on Localization and GNSS (ICL-GNSS), Barcelona, Spain, 28–30 June 2016.
24. Kulmer, J.; Leitinger, E.; Grebien, S.; Witrisal, K. Anchorless Cooperative Tracking Using Multipath Channel Information. *IEEE Trans. Wirel. Commun.* **2018**, *17*, 2262–2275. [CrossRef]
25. DW1000 User Manual. Available online: https://www.decawave.com/sites/default/files/resources/dw1000_user_manual_2.11.pdf (accessed on 10 November 2019).
26. Zhang, R.; Hoflinger, F.; Reindl, L. Inertial Sensor Based Indoor Localization and Monitoring System for Emergency Responders. *IEEE Sens. J.* **2013**, *13*, 838–848. [CrossRef]
27. Kulmer, J.; Leitinger, E.; Meissner, P.; Hinteregger, S.; Witrisal, K. An Alternative Double-Sided Two-Way Ranging Method. In Proceedings of the 2016 13th Workshop on Positioning, Navigation and Communications (WPNC), Bremen, Germany, 19–20 October 2016.
28. Bottigliero, S.; Milanese, D.; Saccani, M.; Maggiora, R. A Low-Cost Indoor Real-Time Locating System Based on TDOA Estimation of UWB Pulse Sequences. *IEEE Trans. Instrum. Meas.* **2021**, *70*, 1–11. [CrossRef]

29. Kay, S.M. *Fundamentals of Statistical Signal Processing: Estimation Theory*; Oppenheim, A.V., Eds.; Technometrics: Upper Saddle River, NJ, USA, 1993; p.50.
30. Shen, Y.; Win, M.Z. Fundamental Limits of Wideband Localization— Part I: A General Framework. *IEEE Trans. Inf. Theory* **2010**, *56*, 4956–4980. [[CrossRef](#)]
31. Huang, Y.; Li, Q.; Ma, W.; Zhang, S. Robust Multicast Beamforming for Spectrum Sharing-Based Cognitive Radios. *IEEE Trans. Signal Process.* **2012**, *60*, 527–533. [[CrossRef](#)]